

Two-Dimensional Analytical Threshold Voltage Modelling of Pseudomorphic Si_{0.8}Ge_{0.2} *p*-Channel MOSFETs

G. ANSARIPOUR*

Department of Physics, Yazd University, P.O. Box 89195-741, Yazd, Iran

(Received April 13, 2009; in final form June 10, 2011)

In this work we present an analytical model of the threshold voltage of SiGe *p*-channel metal oxide semiconductor field effect transistor based on the solution of the two-dimensional Poisson's equation and the ground state wave function of Fang and Howard, and taking into account the space charge in the channel and its effect on the surface potential. It is seen that the experimental data are well fitted within the experimental error that shows the appropriateness of the implemented model. Also comparing the calculated results to that of the calculated from the available recent reported models indicates a reasonable improvement to them.

PACS: 73.23.-b

1. Introduction

Hot-carrier effects (HCEs) should inevitably be taken into account as the dimension of metal oxide semiconductor field effect transistors (MOSFETs) are shrank into nanoscale regime. Regarding HCEs, MOSFETs and heterostructure devices have considerably been studied and modelled [1–6]. It is well known that threshold voltage is MOSFET's important characteristic and there have been many efforts to analytically model the threshold voltage for MOSFETs, particularly for short channel transistors [7–14]. An accurate model is required to predict the threshold voltage. However this is not an easy task to deal with if the channel length of the device is reduced because the depletion width of the source and drain becomes comparable with the channel length.

A short channel threshold voltage based on the analytical solution of the two-dimensional Poisson (2D) equation has been derived [15]. This reference assumed a rather constant charge distribution on the right hand side of Poisson's equation. This appears not to be an actual assumption due to the complexity of the charge distribution at the channel. However a realistic treatment of the energy band structure must take into account the space charge in the channel and its effect on the surface potential.

In this article we propose an accurate analytical model for the threshold voltage via solving the two-dimensional (2D) Poisson equation by taking into account the ground state wave function of Fang and Howard and the space charge in the channel and its effect on the surface potential.

2. Fabrication procedure

The SiGe devices were fabricated from solid-source molecular beam epitaxy (MBE) material grown in a VG

Semicon V905 MBE system. Each sample consists of 300 nm undoped Si buffer on a (100) oriented (2–10 Ω cm) *n*-type Si substrate followed by a 20 nm SiGe layer and 7 nm Si cap.

To avoid relaxation of the strained SiGe layer, the processing was performed at a temperature of 750 °C or below. Two types of gate oxide are used in the study: (1) a plasma grown oxide at low temperature (< 300 °C). (2) A low pressure chemical vapour deposition (LPCVD) oxide deposited at 400 °C. Details of the oxide characteristics and growth process are given by Kennedy et al. [16] and Goh et al. [17]. To make the poly-Si gate and channel electrically conducting at all temperatures, a single 20 keV BF₂ implant was used at a dose of 1 × 10¹⁶ cm⁻². A detailed study of this structure is given elsewhere [18].

3. Theoretical model

In this work the ground state wave function of Fang and Howard [19] is used as they suggested in their work of electron inversion layer in Si MOSFET's

$$g(z) = \left[\frac{b^3}{2} \right]^{1/2} z e^{-bz/2}, \quad (1)$$

in which

$$b = \left[\frac{48m^*e^2}{\hbar^2\varepsilon_{\text{Si}}} \left(N_{\text{dep}} + \frac{11}{32}N_s \right) \right]^{1/3}, \quad (2)$$

where z is the width of the quantum well, b is a variational parameter, N_{dep} is the sheet density of depleted background *n*-type impurities, m^* is the effective mass, e is the electronic charge, \hbar is the Planck constant, ε_{Si} is the dielectric of silicon film and N_s is the carrier sheet density.

First Poisson's equation is analytically solved in two dimensions using a constant charge distribution of carriers,

$$\frac{\partial^2\psi}{\partial x^2} + \frac{\partial^2\psi}{\partial y^2} = \frac{eN_d}{\varepsilon_{\text{Si}}}, \quad (3)$$

where ψ is the electrostatic potential, N_d is the substrate

* e-mail: gansaripour@yazduni.ac.ir

doping concentration. The boundary conditions that we use are the same as used by [15] and are as follows:

$$\psi(x, 0) - \frac{t_{\text{ox}}\varepsilon_{\text{Si}}}{\varepsilon_{\text{ox}}} \frac{\partial\psi}{\partial y}(y=0) = V_g - V_{\text{fb}} = V_{\text{gm}}, \quad (4)$$

$$\psi(0, y) = V_{\text{bi}}, \quad (4a)$$

$$\psi(L, y) = V_{\text{bi}} + V_{\text{ds}}, \quad (4b)$$

$$\frac{\partial\psi}{\partial y}(y=d) = 0, \quad (4c)$$

where t_{ox} , ε_{ox} , V_g , V_{fb} , V_{ds} and V_{bi} are oxide thickness, oxide dielectric, gate voltage, flat-band voltage, drain voltage and built in voltage, respectively. Poisson's equation,

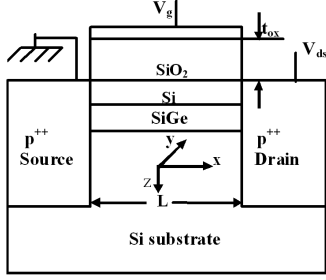


Fig. 1. Cross-sectioned schematic of a p -channel MOS-FET used in this work.

i.e. Eq. (3), in two dimensions is solved subjected to the boundary conditions of Eq. (4), using the separation of variable technique (see Fig. 1), then $\psi(x, y)$ can be shown as [15]:

$$\psi(x, y) = \sum_{n=0}^{\infty} \frac{\cos \gamma_n(y-d)}{\sinh \gamma_n L} [C_n \sinh \gamma_n(L-x) + C'_n \sinh \gamma_n x] + \phi_p, \quad (5)$$

where

$$\phi_p = -\frac{Ky(2d-y)}{2} - \frac{Kt_{\text{ox}}d\varepsilon_{\text{Si}}}{\varepsilon_{\text{ox}}} + V_{\text{gm}}, \quad (6)$$

$$K = \frac{eN_d}{\varepsilon_{\text{Si}}}, \quad (7)$$

$$C_n = \frac{\sin \gamma_n d}{\alpha_n \gamma_n d} \left(V_{\text{bi}} - V_{\text{gm}} + \frac{K}{\gamma_n^2} \right), \quad (8)$$

$$C'_n = \frac{\sin \gamma_n d}{\alpha_n \gamma_n d} \left(V_{\text{ds}} + V_{\text{bi}} - V_{\text{gm}} + \frac{K}{\gamma_n^2} \right), \quad (9)$$

$$\alpha_n = \frac{1}{2} + \frac{1}{4} \frac{\sin 2\gamma_n d}{\gamma_n d}, \quad (10)$$

$$\gamma_n d = \tan^{-1} \left(\frac{\varepsilon_{\text{ox}}}{t_{\text{ox}} \gamma_n \varepsilon_{\text{Si}}} \right) + n\pi, \quad n = 0, 1, 2, \dots \quad (11)$$

In this section, we rewrite Poisson's equation regarding the ground state wave function of Fang and Howard [19] (Eq. (1)):

$$\frac{\partial^2 \psi}{\partial x^2} + \frac{\partial^2 \psi}{\partial y^2} = K'y^2 e^{-by}, \quad (12)$$

where

$$K' = \frac{eN_s b^3}{\varepsilon_{\text{Si}} 2}. \quad (13)$$

Using Eq. (4), it can be shown that $\psi(x, y)$ is as follows:

$$\psi(x, y) = \sum_{n=0}^{\infty} \frac{\cos \gamma_n(y-d)}{\sinh \gamma_n L} [F_n \sinh \gamma_n(L-x) + F'_n \sinh \gamma_n x] + \phi_p \quad (14)$$

in which

$$\phi_p = \frac{K'}{b^2} \left(y^2 + \frac{4y}{b} + \frac{4}{b^2} \right) e^{-by} + K_1 y + K_2, \quad (14a)$$

$$K_1 = \frac{K'}{b^2} e^{-bd} \left(d^2 + \frac{2d}{b} + \frac{2}{b^2} \right), \quad (14b)$$

$$K_2 = V_{\text{gm}} - \frac{4K'}{b^4} + \frac{t_{\text{ox}}\varepsilon_{\text{Si}}}{\varepsilon_{\text{ox}}} \left(-\frac{2K'}{b^3} + K_1 \right), \quad (14c)$$

$$F_n = \frac{1}{\alpha_n \sinh \gamma_n L} \left[\frac{\sinh \gamma_n d}{\gamma_n d} \left(V_{\text{bi}} - A_n \gamma_n - \frac{B_n t_{\text{ox}} \gamma_n^2 \varepsilon_{\text{Si}}}{\varepsilon_{\text{ox}}} \right) - \frac{D_n}{d} \right], \quad (14d)$$

$$F'_n = \frac{1}{\alpha_n \sinh \gamma_n L} \left[\frac{\sinh \gamma_n d}{\gamma_n d} \left(V_{\text{bi}} + V_{\text{ds}} - A_n \gamma_n - \frac{B_n t_{\text{ox}} \gamma_n^2 \varepsilon_{\text{Si}}}{\varepsilon_{\text{ox}}} \right) - \frac{D_n}{d} \right], \quad (14e)$$

$$B_n = RK_p \left(2bR^2(b^2 - 3\gamma_n^2) + \frac{4R}{b} \times (b^2 - \gamma_n^2) + \frac{4}{b} \right) - \frac{K_1}{\gamma_n^2}, \quad (14f)$$

$$A_n = 2RK_p \gamma_n \left(R^2(3b^2 - \gamma_n^2) + 4R + \frac{2}{b^2} \right) + \frac{K_2}{\gamma_n}, \quad (14g)$$

$$D_n = -RK_p e^{-bd} \left[2bR^2(b^2 - 3\gamma_n^2) + 2R(b^2 - \gamma_n^2) \times \left(d + \frac{2}{b} \right) + \left(bd^2 + 4d + \frac{4}{b} \right) \right] + \frac{K_1}{\gamma_n^2}, \quad (14h)$$

$$R = \frac{1}{b^2 + \gamma_n^2}, \quad (14i)$$

$$K_p = \frac{K'}{b^2}, \quad (14j)$$

where α_n and $\gamma_n d$ are given by Eqs. (10) and (11). At distance $x = x_0$ from the source, the minimum surface potential occurs at the threshold and this is twice of the Fermi potential, i.e., $\psi(x_0, 0) = 2\phi_f$.

From Eqs. (4, 4a-4c) and the threshold condition, one has

$$V_{\text{th}} - V_{\text{fb}} = 2\phi_f - \frac{t_{\text{ox}}\varepsilon_{\text{Si}}}{\varepsilon_{\text{ox}}} \frac{\partial\psi}{\partial y}(x=x_0, y=0). \quad (15)$$

Using Eqs. (14, 14a-14j), it can be shown that the threshold voltage, i.e. Eq. (15) would be

$$V_{\text{th}} = V_{\text{th0}} - \frac{t_{\text{ox}}\varepsilon_{\text{Si}}}{\varepsilon_{\text{ox}}} \left\{ \sum_{n=0}^{\infty} \frac{\sin \gamma_n d}{\sinh \gamma_n L} \right.$$

$$\times [F_n \sinh \gamma_n (L - x_0) + F'_n \sinh \gamma_n x_0] + K_1 \Big\}, \quad (16)$$

where $V_{th0} = V_{fb} + 2\phi_f + \frac{eN_d t_{ox}}{\epsilon_{ox}}$ represents the long-channel threshold voltage. A comparison between the threshold voltages calculated from this work with the available reported results is given below.

The first V_{th} model used in this work for comparison is given by [12, 20–22]:

$$V_{th} = V_{th1} - \sigma V_{ds}, \quad (17)$$

$$V_{th1} = V_{fb} + \phi(0) - F \frac{qN_B}{C_{ox}} t_{dmax}, \quad (17a)$$

$$\phi(0) = 2\phi_f + \Delta E_v/q, \quad (17b)$$

$$\phi_f = -\frac{kT}{q} \ln(N_{ch}/n_i), \quad (17c)$$

$$F = 1 - \frac{x_j}{L} \left(\sqrt{1 + \frac{2t_{dmax}}{x_j}} - 1 \right), \quad (17d)$$

$$t_{dmax} = -t_{SiGe} + \sqrt{t_{SiGe}^2 - \frac{2\epsilon_{Si}}{qN_B} \phi(0)}, \quad (17e)$$

$$\sigma = \frac{\epsilon_0 \epsilon_{SiGe}}{\pi C_{ox} L^3}, \quad (17f)$$

$$\epsilon_{SiGe}(y) = 11.9 + 4.1y, \quad (17g)$$

where ϕ_f , V_{fb} , F , x_j , σ , ϵ_{SiGe} are the Fermi potential in the SiGe-channel, flat-band voltage, charge sharing factor, junction depth of source/drain region, DIBL factor [21], relative permittivity of $Si_{1-y}Ge_y$ strained layer [22], respectively, and $C_{ox} = \epsilon_{ox}/t_{ox}$. All other parameters in Eqs. (17, 17a–17g) are the same as given in Ref. [12].

In the above model the short channel effect (SCE) which reduces threshold voltage has been considered. Using Eqs. (17, 17a–17g) the calculated results are given in Fig. 3b (dashed line) [12].

The second V_{th} model used in this work for comparison is given as [13]:

$$V_{th} = V_{fb} + \gamma_s + \sqrt{\phi_{s0} - V_{bs}} \left[1 - \frac{\lambda \zeta}{L_{eff}} \left(\sqrt{\phi_{s0} - V_{bs}} + \frac{V_{bs}}{\sqrt{\phi_{s0} - V_{bs}}} \right) \right], \quad (18)$$

$$\zeta = \sqrt{\frac{2\epsilon_{Si}}{qN_{eff}}}, \quad (18a)$$

$$\phi_{s0} = \frac{2kT}{q} \ln \left(\frac{N_{eff}}{n_i} \right) \sqrt{\phi_{s0} - V_{bs}}, \quad (18b)$$

$$\phi_s = \phi_{s0} - \Delta\phi_s, \quad (18c)$$

$$\Delta\phi_s = \frac{1}{\cosh \left(\frac{L_{eff}}{2l_\alpha} \right)} \left[(V_{bi} - \phi_{s0}) \cosh \left(\frac{z}{2} \right) \right]$$

$$+ \frac{i v_{ds}}{2} \frac{\sinh \left(\frac{L_{eff}}{2l_\alpha} - \frac{z}{2} \right)}{\sinh \left(\frac{L_{eff}}{2l_\alpha} \right)}, \quad (18d)$$

$$I_\alpha = \alpha (\phi_{s0} - V_{bs})^{0.25}, \quad (18e)$$

$$I_\beta = \beta (\phi_{s0} - V_{bs})^{0.25}, \quad (18f)$$

$$z = \ln \left(\frac{V_{bi} - \phi_{s0} + V_{ds}}{V_{bi} - \phi_{s0}} \right). \quad (18g)$$

All other parameters in Eqs. (18, 18a–18g) are the same as given in Ref. [13]. Using Eqs. (18, 18a–18g) the calculated results are given in Fig. 3b (dash-dotted line) [13]. The constants used in the calculations are given in Table.

Parameters used in the calculations. TABLE

hole effective mass	$m^* = 0.23m_0$ [23]
depleted background impurities	$N_{dep} = 5 \times 10^{16} \text{ cm}^{-2}$ [6, 18]
substrate doping	$N_d = 1 \times 10^{15} \text{ cm}^{-3}$ [6, 18]
built in voltage	$V_{bi} = -0.5 \text{ V}$
flat band voltage	$V_{fb} = -0.45 \text{ V}$
minimum length of channel depletion	$d = 2 \text{ }\mu\text{m}$
oxide layer thickness	$t_{ox} = 190 \text{ nm}$ [6, 18]
dielectric of oxide layer	$\epsilon_{ox} = 3.9\epsilon_0$
dielectric of Si film	$\epsilon_{Si} = 11.9\epsilon_0$
thickness of SiGe film	$t_{SiGe} = 27 \text{ nm}$ [6, 18]
junction depth of source/drain	$x_j = 1 \text{ }\mu\text{m}$
Ge content	$y = 0.2$
peak pile-up doping concentration	$N_{pile} = 2 \times 10^{17} \text{ cm}^{-3}$ [13]

4. Calculated results and discussion

Using Eq. (14), the surface potential variation along the devices against the effective channel length is plotted in Fig. 2. For all devices used in this work we have performed shift and ratio method to extract the effective channel length [4].

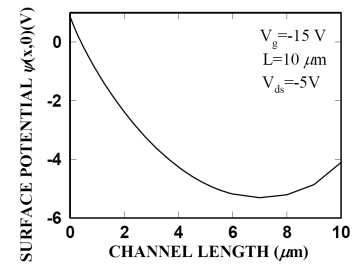


Fig. 2. Variation of the surface potential along with the channel length.

This figure shows that for the device with effective channel length of $8 \text{ }\mu\text{m}$, the surface potential is not constant over the entire channel (except between $6 \text{ }\mu\text{m}$ to $8 \text{ }\mu\text{m}$ which changes slowly). This result shows the inappropriateness of ignoring the space charge in the channel. In case of the device with $2 \text{ }\mu\text{m}$ effective channel length,

a large variation along the channel is seen as expected from the 2D analysis.

Using Eq. (16), the calculated threshold voltage (solid line) is depicted in Fig. 3a along with our measured threshold voltage (white circle) of different p -channel lengths of $\text{Si}_{0.8}\text{Ge}_{0.2}$ MOSFETs [4, 14, 23].

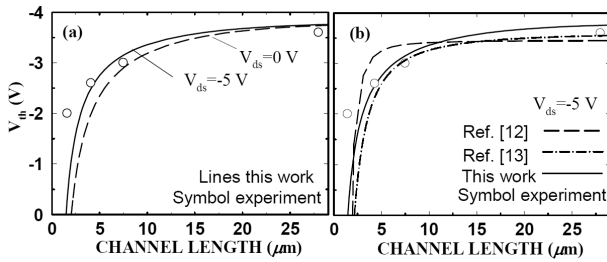


Fig. 3. Threshold voltage vs. effective channel length for (a) drain voltage, V_{ds} of 0 and -5 V along with the experimental results and (b) the same as (a) but the calculated results of the two models [12, 13] have been added.

Figure 3b is the same as Fig. 3a but, for comparison we have added the results of the calculations using Eqs. (17, 17a–17g [12]) (long dashed line) and Eqs. (18, 18a–18g [13]) (dash-dotted line).

Figure 3b shows that the measured threshold voltages over the short channel devices ranging from 1.5 to 8.5 μm begins to rise at a rate smaller than the calculated results (long-dashed line) of model [12] can account for, but this is not the case (except for the shortest channel device of 1.5 μm) for the two other solid and dash-dotted lines calculated in work and according to the model [13], respectively.

However, our calculated results (solid line in Fig. 3b) based on the work given in this paper seems to fit the experimental data reasonably better, over the entire range, than that of the calculated results based on Ref. [13] (dash-dotted line in Fig. 3b). This might be attributed to taking account the ground state wave function in our proposed model in this work that affects the short channel devices [24].

5. Conclusion

To conclude we have presented an analytical model for the threshold voltage of $\text{Si}_{0.8}\text{Ge}_{0.2}$ p -MOSFETs based on the ground state wave function of Fang and Howard and explicit solution of 2D Poisson's equation taking account the space charge in the channel. It is seen that the experimental data is well fitted which indicates the suitability of the implemented model, particularly for relatively shorter channel devices. Moreover, a comparison has been made between the calculated results of our implemented model to that of two other models demonstrating the relative superiority of the presented model that incorporates the ground state wave function in the channel.

References

- [1] Y.-S. Jean, C.-Y. Wu, *IEEE Trans. Electron Dev.* **44**, 441 (1997).
- [2] G. Braithwaite, N. Matthey, E.H.C. Parker, T.E. Whall, E. Brunthaler, G. Bauer, *J. Appl. Phys.* **81**, 68531 (1997).
- [3] S. Kaya, Y.-P. Zhao, J.R. Waiting, A. Asenov, J.R. Barker, G. Ansaripour, G. Braithwaite, T.E. Whall, E.H.C. Parker, *Semicond. Sci. Technol.* **5**, 573 (2000).
- [4] G. Ansaripour, G. Braithwaite, S. Agan, T.E. Whall, E.H.C. Parker, *Microelectron. Eng.* **51-52**, 541 (2000).
- [5] G. Ansaripour, *Thin Solid Films* **517**, 6105 (2009).
- [6] G. Ansaripour, *Thin Solid Films* **518**, 5599 (2010).
- [7] J.A. Greenfield, R.W. Dutton, *IEEE Trans. Electron. Dev.* **ED-27**, 1520 (1980).
- [8] R.R. Troutman, S.N. Chakravart, *IEEE Trans. Cir. Theor.* **CT-20**, 659 (1973).
- [9] H. Masuda, M. Nakai, R. Hori, M. Kobo, *Trans. IEEE Japan* **60-C**, 205 (1977).
- [10] S. Baishya, A. Mallik, C.K. Sarkar, *Microelectron. Reliability* **48**, 17 (2008).
- [11] W. Wu, R. Yao, X. Zheng, *Solid-State Electron.* **53**, 907 (2009).
- [12] X. Zou, J.P. Xu, C.X. Lee, P.T. Lai, W.B. Chen, *Microelectron. Reliability* **47**, 391 (2007).
- [13] K.-Y. Lim, X. Zhou, Y. Wang, *J. Model. Simul. Microstruct.* **2**, 51 (1999).
- [14] G. Ansaripour, *Recent Res. Dev. Sci. Tech. Semicond.* **1**, 51 (2003).
- [15] D.R. Poole, D.L. Kwong, *IEEE Electron. Dev. Lett.* **EDL-5**, 443 (1984).
- [16] G.P. Kennedy, S. Taylor, W. Eccleston, W.M. Arnold-bik, F.H.P.M. Habraken, *Microelectron. Eng.* **25**, 141 (1984).
- [17] I.S. Goh, J.F. Zhang, S. Hall, W. Eccleston, K. Werner, *Semicond. Sci. Technol.* **10**, 818 (1995).
- [18] R.J.P. Lander, C.J. Emeleus, B.M. McGregor, E.H.C. Parker, T.E. Whall, A.G.R. Evans, G.P. Kennedy, *J. Appl. Phys.* **82**, 5210 (1997).
- [19] F.F. Fang, W.E. Howard, *Phys. Rev. Lett.* **16**, 797 (1966).
- [20] L.D. Yau, *Solid-State Electron.* **17**, 1059 (1974).
- [21] N.D. Arora, L.M. Richardson, *MOSFET Modelling for Circuit Simulation: Advanced Device Physics*, Academic Press Inc., New York 1989.
- [22] H.M. Nayfeh, H. Hoyt, D.A. Antoniadis, *IEEE Trans. Electron. Dev.* **51**, 2069 (2004).
- [23] G. Ansaripour, G. Braithwaite, M. Myronov, O.A. Mironov, E.H.C. Parker, T.E. Whall, *Appl. Phys. Lett.* **76**, 1140 (2000).
- [24] M.A. Sadeghzadeh, A.I. Horrell, O.A. Mironov, E.H.C. Parker, T.E. Whall, M.J. Kearney, *Appl. Phys. Lett.* **76**, 2568 (2000).